THE JOURNAL OF PHYSICAL CHEMISTRY A
A JOURNAL OF THE AMERICAN CHEMICAL SOCIETY

pubs.acs.org/JPCA

Article

Singlet O_2 from Ultraviolet Excitation of the Quinoline-O_2 Complex

Bradley F. Parsons,* Marcos R. Rivera, Mark A. Freitag, Kylie A. Reardon, Emerson S. Pappas, and Jack T. Rausch

Cite This: *J. Phys. Chem. A* 2023, 127, 4957−4963

Read Online

ACCESS | Metrics & More | Article Recommendations | Supporting Information

ABSTRACT: We report results from experiments with the quinoline-O_2 complex, which was photodissociated using light near 312 nm. Photodissociation resulted in formation of the lowest excited state of oxygen, O_2 a $^1\Delta_g$, which we detected using resonance enhanced multiphoton ionization and velocity map ion imaging. The O_2^+ ion image allowed for a determination of the center-of-mass translational energy distribution, $P(E_T)$, following complex dissociation. We also report results of electronic structure calculations for the quinoline singlet ground state and lowest energy triplet state. From the CCSD/aug-cc-pVDZ//(U)MP2/cc-pVDZ calculations, we determined the lowest energy triplet state to have $\pi\pi^*$ electronic character and to be 2.69 eV above the ground state. We also used electronic structure calculations to determine the geometry and binding energy for several quinoline-O_2 complexes. The calculations indicated that the most strongly bound complex has a well depth of about 0.11 eV and places the O_2 moiety above and approximately parallel to the quinoline ring system. By comparing the experimental $P(E_T)$ with the energy for the singlet ground state and the lowest energy triplet state, we concluded that the quinoline product was formed in the lowest energy triplet state. Finally, we found the experimental $P(E_T)$ to be in agreement with a Prior translational energy distribution, which suggests a statistical dissociation for the complex.

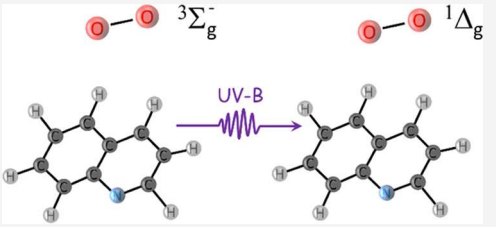

I. INTRODUCTION

Quinoline is a mono-substituted azanaphthalene that exhibits essentially no fluorescence following ultraviolet excitation to the lowest lying singlet states. In solution quinoline shows ultraviolet absorption bands with two maxima near about 275 nm and about 313 nm.[1−3] These maxima shift with solvent and are assigned as transitions to $\pi\pi^*$ excited singlet states.[3] In the most recent gas phase absorption spectrum,[4] these transitions were observed as a narrow band at 3.99 eV (311 nm) and as a broad band centered near 4.71 eV (263 nm). The former transition is assigned as the 2 ^{1}A′ ← 1 ^{1}A′ ($\pi\pi^*$) transition and the latter as the 3 ^{1}A′ ← 1 ^{1}A′ ($\pi\pi^*$) with the origin bands for these states at 3.991 and 4.441 eV, respectively.[4−6] Based on the 1+1′ resonance enhanced multiphoton ionization (REMPI) spectrum of quinoline, the ($n\pi^*$) excited state is slightly lower in energy at 3.77 eV (334 nm).[5,6] Finally, the lowest energy quinoline ($\pi\pi^*$) triplet state lies near 2.79 eV based on the gas phase luminescence spectrum.[5,7]

For quinoline, the maximum fluorescence to phosphorescence ratio is F/P ∼ 2 × 10^{-5} based on the lower detection limit from the observed combined luminescence spectrum.[2] The weak fluorescence and strong phosphorescence results from efficient intersystem crossing that has been attributed to spin-orbit coupling along with vibronic coupling in the triplet manifold allowing phosphorescence to gain intensity.[8] More recent electronic structure calculations also confirm quinoline to have strong spin-orbit coupling between the singlet and triplet manifolds compared with the related aza-compounds: isoquinoline, indole and isoindole, although we note this study focused on intersystem crossing from the lowest energy ($n\pi^*$) singlet state.[9]

Quinoline also forms the central ring system for quinolone and the associated fluoroquinolone antibiotics and these antibiotics are known to cause phototoxicity.[10] Antibiotic and pharmaceutical phototoxicity is a concern in clinical settings as well as more generally since these antibiotics have been observed in environmental water studies.[11,12] Fluoroquinolone phototoxicity may be attributed to formation of either F^- or reactive oxygen species such as superoxide, O_2^-, or singlet oxygen: $^1O_2$ (a $^1\Delta_g$).[13,14] These reactive oxygen species may be formed through a photosensitization reaction between O_2 and an excited photosensitizer and for fluoroquinolones the observed solution phase $^1O_2$ quantum yield, Φ_Δ, varies with derivatization.[14] We also note that while $^1O_2$ may account for some of the observed fluoroquinolone phototoxicity, $^1O_2$ has beneficial uses including photodynamic therapy cancer treatments[15] and point-of-use water disinfection.[16] As such, we are interested in $^1O_2$ formation and the current work seeks to better understand the intrinsic photochemistry of the quinoline-O_2 complex and thus provide a baseline for future studies.

Received: March 27, 2023
Revised: May 5, 2023
Published: June 1, 2023

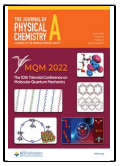

https://doi.org/10.1021/acs.jpca.3c02024
J. Phys. Chem. A 2023, 127, 4957−4963

Gas phase experiments with the isoprene-O_2 complex observed $^1O_2$ following ultraviolet excitation, and this product was assigned to a double spin flip (DSF) process.[17] This field was recently reviewed by Baklanov and Parker,[18] and during the DSF transition, both moieties of a complex undergo spin-changing transitions but the overall complex multiplicity is unchanged. For quinoline-O_2 the DSF transition may be written as $^3(^1Q–^3O_2) \rightarrow {}^3(^3Q^*–^1O_2)$, where ^1Q and $^3Q^*$ are the quinoline singlet ground state and lowest triplet excited states, respectively. The DSF transition energy may be estimated[17] as the triplet state energy and the $^1O_2$ term energy, 0.98 eV.[19] Using the quinoline triplet energy of 2.79 eV,[7] we expect the threshold for the DSF transition to be about 3.87 eV when accounting for the complex binding energy of about 0.1 eV. While a vertical transition would be somewhat higher in energy, we expect this threshold transition may be accessible at 312 nm (3.97 eV) and in Figure 1, we have

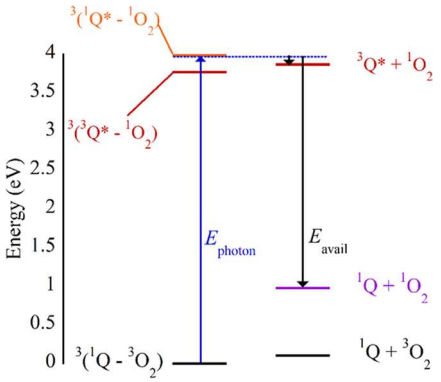

Figure 1. Schematic energy diagram for excited state and product channels resulting in $^1O_2$. At 3.97 eV, the available transitions include: DSF (red line) or locally excited quinoline (orange line). The blue upward arrow corresponds to the above photon energy. The available product channels are shown on the right and differ by the quinoline triplet state energy, 2.79 eV. The downward black arrows correspond with the available energy that may be partitioned into CM translation and quinoline vibrational excitation.

indicated the DSF transition energy as the horizontal red line. An organic-O_2 complex may also potentially undergo a charge transfer transition between the organic donor and O_2 acceptor.[20] The approximate threshold energy for a charge transfer transition may be estimated as: $E_{CT} = IP_D - EA_A - e^2/R$,[21] where IP_D is the ionization energy for quinoline, 8.63 eV,[19] EA_A is the O_2 adiabatic electron affinity, 0.448 eV,[22] and R is the point charge separation. While this simplistic calculation suggests the threshold for a charge transfer transition to be around 4 eV, the increased O_2^- bond relative to ground state O_2 results in a vertical transition to the charge transfer state at an energy above 4.3 eV.[22] Thus, we expect this state to be inaccessible at 3.97 eV although a 266 nm photon (4.66 eV) may potentially access the charge transfer state. Finally, since the quinoline absorption spectrum shows a band at 311 nm, we also consider the possibility for localized excitation of the quinoline moiety. Localized excitation may promote quinoline to the lowest $\pi\pi^*$ singlet excited state: $^3(^1Q–^3O_2) \rightarrow {}^3(^1Q^*–^3O_2)$, which is shown by the horizontal orange line in Figure 1.

Figure 1 also depicts the expected energetics for product channels resulting in $^1O_2$ and either ground state quinoline, ^1Q, or the lowest quinoline triplet state, $^3Q^*$. The black vertical arrows in Figure 1 indicate the available energy that may be partitioned into either center-of-mass (CM) recoil kinetic energy or internal energy of the quinoline product. We note the large difference in available energy (2.79 eV) between the $^1Q + {}^1O_2$ and $^3Q^* + {}^1O_2$ product channels can be resolved in our conventional velocity map ion imaging experiments, which are discussed in the next section along with computational methods. In Section III, we then present our computational and experimental results and evaluate the data to determine the product channels from complex dissociation. We also compare the experimental results with that expected for a statistical dissociation using the Prior distribution and we comment on the excited state. Finally, in Section IV, we present a brief conclusion for this study.

II. METHODS

II.I. Theoretical Methods. The relative energies of the quinoline singlet and triplet states are determined using *ab initio* electronic structure calculations carried out with the GAMESS[23] suite of programs while the structure and energetics of the quinoline-O_2 complex are determined using the ORCA program suite.[24] We determine the geometry for the quinoline singlet state with the MP2 method,[25] and for the quinoline triplet state and for the quinoline-O_2 complexes using the UMP2 method.[26] For all structures, geometry optimizations are performed using the correlation consistent double-ζ basis set, cc-pVDZ,[27] and the lowest energy stationary points are confirmed as minima using double differenced numerical Hessian calculations. Finally, using the optimized (U)MP2/cc-pVDZ geometries, we determine the single point energies at both the (U)MP2/aug-cc-pVDZ and CCSD/aug-cc-pVDZ levels of theory.[28]

II.II. Experimental Section. The original quinoline sample (Sigma-Aldrich) was dark from impurities and so we vacuum distill the sample and verify the purity using GCMS. After purification, we measure the vapor pressure above the quinoline to be ~0.3 Torr at 20 °C using a Baratron pressure gauge (MKS), and for experiments we place 30 μL of quinoline inside the quartz sample tube of an Even-Lavie pulsed nozzle (Lamid, 150 μm orifice).[29,30] We back the nozzle with about 200 psig (15 bar) of a gas mix consisting of 3% O_2 in a He buffer. The resulting supersonic expansion is about 20 μs wide and passes through a 3.0 mm diameter skimmer (Beam Dynamics) located about 100 mm downstream from the nozzle. After skimming, the resulting molecular beam passes along the cylindrical axis of a four plate ion optics stack allowing for conventional velocity map ion imaging.[31]

Between the first and second ion optics we cross the molecular beam with light near 312 nm (3.97 eV) generated by frequency doubling the 624 nm output from a Nd:YAG pumped dye laser (Sirah Cobra Stretch). The same laser pulse excites the quinoline-O_2 complex and resonantly ionizes the O_2 a $^1\Delta_g$ state using the two-photon allowed transition to the d $^1\Pi_g$ state.[32−34] The resulting O_2^+ is projected onto a 2D position sensitive detector and the ion image is recorded using a CCD camera (QCam Fast 1394). In the image, individual ions are several pixels wide and this width sets a lower limit for the experimental kinetic energy resolution. To improve this resolution, we event count individual ions by recording short duration (~200 ms) images and we centroid individual images using the Python 3.10 SciKit Imaging libraries. The composite

https://doi.org/10.1021/acs.jpca.3c02024
J. Phys. Chem. A 2023, 127, 4957−4963

event counted image is then Abel inverted using the Basex program.[35]

In the experiment, the VMI ion optics magnify the image such that the observed velocity, v_{obs}, is larger than the actual velocity, v_{actual}, resulting in a magnification factor of $M = v_{obs}/v_{actual}$. We calibrate the experimental magnification factor using the photodissociation of methyl iodide, CH_3I, at 266 nm from a second Nd:YAG laser (Amplitude Surelite EX) and we resonantly ionize the I ($^2P_{3/2}$) and I* ($^2P_{1/2}$) products near 304 nm.[36]

Finally, as with our previous experiments,[32] we record the 2+1 REMPI spectrum for $^1O_2$ by scanning the dye laser wavelength while measuring the total detector signal for m/z = 32. To record the spectrum, the detector signal for a particular mass is binned using a boxcar integrator (Stanford Research Systems SR250) and recorded using a USB data acquisition device (LabJack U3-HV).

III. RESULTS AND DISCUSSION

The geometry for the quinoline singlet ground state and lowest energy triplet state were optimized using (U)MP2/cc-pVDZ calculations and the overall structure is shown in Figure S1 of the Supporting Information. Tables S1 and S2 of the Supporting Information give the optimized bond lengths and angles and Tables S3 and S4 give the unscaled harmonic vibrational frequencies. Figures S2 and S3 of the Supporting Information show the singly occupied molecular orbitals for the lowest energy triplet state corresponding with a $^3(\pi^1\pi^{*1})$ electron configuration, which is consistent with previous work.[37,38] Our CCSD/aug-cc-pVDZ calculations give a quinoline vertical triplet state energy of 3.29 eV while the zero-point corrected adiabatic triplet state energy was determined to be 2.69 eV, which is 0.1 eV lower than the experimental value of 2.79 eV from the gas phase luminescence spectrum.[7] These values are summarized below in Table 1 and additional computational details are given in the Supporting Information.

Table 1. Triplet State Energy and Cluster Binding Energies

	(U)MP2/aug-cc-pVDZ[a]	CCSD/aug-cc-pVDZ[a]
vertical triplet energy	3.940	3.293
adiabatic triplet energy	3.543	2.823
adiabatic triplet energy + ZPE	3.411	2.692
above ring[b]	0.157	0.110
C-atom side complex[b]	0.078	0.067
N-atom side complex[b]	0.078	0.064

[a]Energy in eV. [b]Labels given in the Supporting Information.

We also optimized the quinoline-O_2 complex geometry and three stable minima were located. Further details of these calculations are given in the Supporting Information and Figure S1 shows the approximate geometries for the three minima. Tables S5−S10 of the Supporting Information give the Cartesian coordinates of the complexes. From these complexes, we determined the binding energy and the results are given in Table 1, which shows the most strongly bound complex has a binding energy of 0.11 eV.

In our experiments, the quinoline-O_2 complex is excited at 312 nm and then dissociates giving the $^1O_2$ product. We first verified the $^1O_2$ product by recording the 2+1 REMPI spectrum using the d $^1\Pi_g$ ($v'' = 3$) ←← a $^1\Delta_g$ ($v'' = 0$) transition.[33,34] In Figure 2 we have compared the experimental spectrum, black points, with a simulated spectrum, red curve,

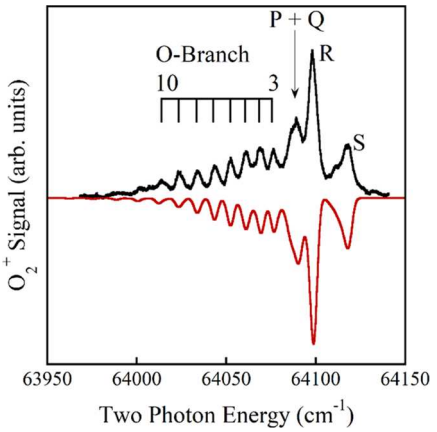

Figure 2. Black points correspond to the observed m/z = 32 (O_2^+) ion signal as a function of two photon energy. The red curve shows the simulated spectrum, which corresponds to an 80 K rotational distribution.

generated using the PGOPHER program.[39] The simulated spectrum has a rotational temperature of 80 K and the simulation reasonably reproduced the experimental spectrum for temperatures ranging between 70 and 90 K. The spectrum in Figure 2 confirms formation of the $^1O_2$ product and we estimate the rotational temperature to be ∼80 ± 10 K corresponding with an average rotational energy of about 7 meV.

We also confirmed formation of the quinoline-O_2 bimolecular complex by recording a mass spectrum of the molecular beam using 312 nm light for non-resonant ionization. Figure S4 of the Supporting information shows the mass spectrum from 90 to 170 u, with peaks at $C_9NH_7^+$ and C_9NH_7-O_2^+. The signal at $C_9NH_7^+$ and C_9NH_7-O_2^+ decreased when the relative timing between the 10 ns laser pulse and the ∼20 μs gas pulse was increased or decreased and both ion signals were maximized within ±3 μs of the middle of the gas pulse. We further note that during all experiments the quinoline vapor pressure was maintained under 0.015 bar and thus constituted less than 0.1% of the total gas mix. Under these conditions, the mass spectrum showed no contribution from higher order clusters and the ion image of the C_9NH_7-O_2^+ signal appeared as a simple beam spot, which indicated the bimolecular complex did not result from dissociation of a higher order cluster.

We recorded the O_2^+ ion image at 312.03 nm, which is the maximum for the R-branch transition in the REMPI spectrum, Figure 2. The ion image appears as the inset of Figure 3 where the vertical arrow indicates the laser polarization.

We used the Basex program[35] to extract the O_2 velocity distribution from the resulting ion image and then transform the velocity distribution to a center-of-mass recoil kinetic energy distribution, $P(E_T)$, accounting for the velocity-to-energy Jacobian.[40] For dissociation of the B-A complex (B = quinoline, A = O_2) the center-of-mass translational energy is given by: $E_T = \left(\frac{m_A + m_B}{m_B}\right)\frac{1}{2}m_A v_A^2$ where m_A and v_A are the mass and velocity of the detected O_2 fragment and the center-of-mass $P(E_T)$ in Figure 3, black points, was determined for dissociation of bimolecular C_9NH_7-O_2.

https://doi.org/10.1021/acs.jpca.3c02024
J. Phys. Chem. A 2023, 127, 4957−4963

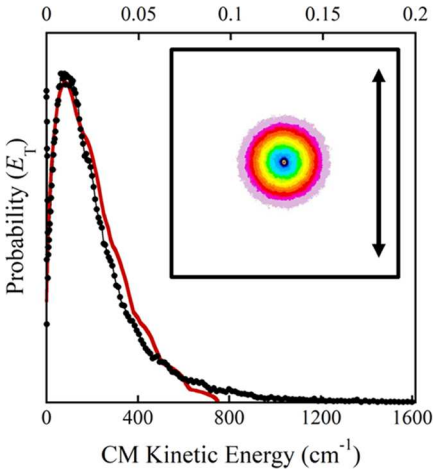

Figure 3. Inset shows the O_2^+ ion image at 3.97 eV (312 nm) photon energy with the vertical arrow indicating the photolysis laser polarization. In the ion image, the O_2^+ signal intensity is a maximum at the center (blue) and decreases moving to the edge (red/light purple region). For the $P(E_T)$, the lower energy axis is in units of cm^{-1} and the upper energy axis is given in units of eV. The black points correspond to the center-of-mass $P(E_T)$ for dissociation of bimolecular C_9NH_7-O_2 and the red curve corresponds to the statistical Prior distribution: P^0 $(E_T|E_{avail})$.

The $P(E_T)$ in Figure 3 extends to a maximum kinetic energy of about 1100 cm^{-1} or 0.13 eV. In the experiment, the photon energy, E_{photon}, dissociates the complex C_9NH_7-O_2 and so some of the photon energy must be used to overcome the complex binding energy, D''. During dissociation, the photon energy is also partitioned into internal energy of the quinoline and $^1O_2$ products, $E_{Q,int}$ and $E_{O_2,int}$, respectively, as well as into center-of-mass translation for the recoiling fragments, E_T. The $^1O_2$ internal energy is the term energy, 0.98 eV, plus the rotational energy, and the latter is essentially zero for the lowest rotational levels probed at the R branch maximum. Thus, the maximum available energy, E'_{avail}, that may be partitioned into either center-of-mass translation, E_T, or quinoline internal energy, $E_{Q,int}$ is then given by:

$$E'_{avail} = E_T + E_{Q,int} = E_{Q,rovib} + E_{Q,el} + E_T = E_{photon} - E_{O_2,int} - D'' \quad (1)$$

Thus, for our 3.97 eV photon, E'_{avail} is 2.88 eV, assuming a binding energy of 0.11 eV for the most strongly bound complex in Table 1. From eq 1, the quinoline internal energy is thus related to the available energy, E'_{avail}, as:

$$E_{Q,int} = E_T - E'_{avail} \quad (2)$$

So, for a maximum kinetic energy of 0.13 eV the minimum quinoline internal energy would be 2.75 eV from eq 2. Moreover, using the normalized experimental $P(E_T)$, Figure 3, we determined the average translational energy as: $E_{T,ave} = \int E_T P(E_T) dE_T$. For quinoline-$O_2$, the average translational energy is 0.032 eV and eq 2 gives the average quinoline internal energy to be 2.848 eV. We summarize these average experimental values in Table 2.

We now compare the experimentally observed quinoline internal energy with that expected for formation of either the ground or triplet excited state. First, ground state quinoline would have a minimum internal energy of 0 eV for vibrationally cold products, which would correspond with a maximum translational energy of 2.88 eV. While we expect vibrational excitation during dissociation, the experimental $P(E_T)$ extending to only 0.13 eV is inconsistent with ground state quinoline. Alternatively, the average quinoline internal energy of about 2.848 eV is only slightly larger than the experimental triplet energy, 2.79 eV, which supports formation of the triplet state. Moreover, while the triplet state energy is slightly greater than the minimum quinoline internal energy from our experiment, 2.75 eV, the latter value was calculated assuming dissociation of the most strongly bound complex with no internal energy before photoexcitation. Dissociation of either (1) a more-weakly bound complex or (2) a complex with significant internal energy before photoexcitation will partition more energy into either CM translation or quinoline internal energy. Either case would increase our calculated minimum internal energy, 2.75 eV, bringing the value into better agreement with the experimental triplet energy. Moreover, partitioning more energy into CM translation would result in a $P(E_T)$ extending beyond the nominal energetic limit and Figure 3 indeed shows a weak tail extending to higher translational energies. A similar high energy tail has been observed in near threshold dissociation of the ArNO complex and was attributed to complexes with significant internal energy before photodissociation (hotbands).[41] Thus, the high energy tail in Figure 3 suggests a contribution from dissociation of more-weakly bound or internally excited quinoline-O_2 complexes.

Table 2. Average Translational and Internal Energies

	$E_{T,ave}$ [a]	$E_{int,ave}$ [a]
experimental	0.032	2.848
prior	0.026	2.854

[a]Energies in eV.

In Figure 3 we also show a Prior distribution P^0 $(E_T|E_{avail})$, which corresponds to a statistical partitioning of available energy, E_{avail}, into CM translation and product rotational and vibrational modes during dissociation.[42,43] Our experiment resonantly ionizes the lowest rotational levels of the $^1O_2$ ground vibrational state and so we only account for the energetically allowed rotational and vibrational modes of quinoline. The available energy for the Prior distribution is: $E_{avail} = E_{Q,rovib} + E_T = E'_{avail} - E_{Q,el}$ with E'_{avail} defined in eq 1. Formation of triplet quinoline results in E_{avail} = 0.09 eV and to find the Prior distribution we use the rotational constants and unscaled harmonic vibrational frequencies from Table S4 of the Supporting Information. The result is given as the red curve in Figure 3 and from the normalized Prior distribution we determined the average translational energy to be 0.026 eV. Using eq 2, this average translational energy corresponds with a predicted average internal energy of 2.854 eV for triplet quinoline and these results are summarized in Table 2.

Figure 3 and Table 2 show excellent agreement between the experimental $P(E_T)$ and that predicted by a Prior distribution corresponding to a statistical partitioning of energy during dissociation. In particular, the quinoline average internal energy is nearly identical, supporting the conclusion that photodissociation of the complex produces triplet quinoline and the $^1O_2$ product. Moreover, as with our previous work with β-ionone-O_2,[32] the close agreement between the experimental $P(E_T)$ and the Prior distribution suggests the complex dissociates statistically.

https://doi.org/10.1021/acs.jpca.3c02024
J. Phys. Chem. A 2023, 127, 4957−4963

We now briefly consider the excited state leading to photodissociation, which must be consistent with formation of $^1O_2$ based on the REMPI spectrum, Figure 2, and must be consistent with the $P(E_T)$ shown in Figure 3. The latter shows that quinoline is formed with a large average internal energy, 2.848 eV, but with a narrow energy distribution since, using eq 2 the internal energy ranges between 2.75 and 2.88 eV. For the DSF excitation, 0.11 eV is partitioned into complex dissociation, 0.98 eV is partitioned to form $^1O_2$ and 2.79 eV is partitioned to form electronically excited triplet quinoline. Again, for an internally cold complex, 0.09 eV remains to be partitioned between CM translation and quinoline rotational and vibrational excitation and this small available energy range would result in a narrow $P(E_T)$ like that observed in Figure 3.

Alternatively, as discussed in the Introduction, 312 nm excitation may also locally excite the quinoline moiety: $^3(^1Q^*-^3O_2)$. Excitation to this locally excited state followed by direct dissociation would yield the $^3O_2$ ground state product, which is inconsistent with our experiments that resonantly ionize $^1O_2$ as shown in Figure 2. Alternatively, vibronic spin-orbit coupling[8] of the quinoline moiety may allow for rapid intersystem crossing from the locally excited state $^3(^1Q^*-^3O_2)$ to the $(^3Q^*-^3O_2)$ complex. Direct dissociation of this complex also yields $^3O_2$, which is again inconsistent with Figure 2. However, analogous to photosensitization, $^3O_2$ may potentially quench the $^3Q^*$ moiety giving ground state quinoline, ^1Q, and the $^1O_2$ product. Such production of $^1O_2$ would be consistent with Figure 2; however, from energy conservation, 2.88 eV must now be partitioned between CM translation and vibrational excitation of ground state quinoline, but Figure 3 extends to at most 0.13 eV of CM translational energy. We briefly considered the ground state quinoline product above, but to further assess this we also determined the Prior distribution for statistical dissociation giving ^1Q and the $^1O_2$ products. Figure S5 of the Supporting Information gives the resulting distribution, which extends to about 1 eV CM translational energy and is thus significantly higher than the maximum observed in Figure 3, ~0.13 eV. Furthermore, the average CM translational energy from the Prior distribution in Figure S5 is 0.17 eV, which is also significantly higher than the experimental value of 0.032 eV, Table 2. Thus, quenching to the ^1Q and $^1O_2$ products through a statistical mechanism cannot account for the experimental $P(E_T)$ in Figure 3 and while a non-statistical quenching mechanism may play a role, we cannot assess this without a better understanding of the quinoline-O_2 excited state.

Another possibility is a concerted intersystem crossing from the locally excited complex: $^3(^1Q^*-^3O_2) \rightarrow {}^3(^3Q^*-^1O_2)$. We refer to this as intersystem crossing although the overall process is spin-allowed. Following such intersystem crossing, direct dissociation of the complex yields the $^1O_2$ and $^3Q^*$ products. Furthermore, since 2.79 eV is partitioned into quinoline electronic excitation, this would result in a narrow CM translational energy distribution and thus be consistent with both Figures 2 and 3. Such an intersystem crossing may potentially be enhanced by the strong quinoline vibronic spin-orbit coupling.[8] However, since either localized excitation followed by intersystem crossing or dissociation through a DSF transition result in the same products our experimental data cannot distinguish between these possible channels. Therefore, a better understanding of these processes would also require high level electronic structure calculations for the complex excited state or perhaps a time-resolved experiment to identify changes in the occupied molecular orbitals.

In order to further consider localized excitation of the quinoline moiety, we also attempted to photolyze the complex at 266 nm (4.66 eV), which is on resonance with a $\pi\pi^*$ higher quinoline excited state.[4] We note that this photon energy may also potentially access a charge transfer state, which as discussed in the Introduction, would have a vertical excitation energy above 4.3 eV. In this final experiment, we first confirmed spatial overlap of the 266 and ~310 nm probe laser through photolysis of CH_3I. However, in the experiment we observed no enhancement to the $^1O_2$ signal due to the 266 nm laser. Moreover, the resulting $P(E_T)$ was identical with that shown in Figure 3, consistent with photolysis at 312 nm. This experiment seems to indicate that the higher energy $\pi\pi^*$ quinoline excited state and the charge transfer state do not play a significant role in $^1O_2$ production.

Finally, our current experiments demonstrate that ultraviolet excitation of the quinoline-O_2 complex directly yields $^1O_2$. This observation of photochemical $^1O_2$ formation may explain some of the observed phototoxicity for the related fluoroquinolone antibiotics and we are interested in future photochemical studies involving derivatized quinoline or fluoroquinolones also complexed with molecular oxygen.

IV. CONCLUSIONS

Using electronic structure calculations, we determined the zero-point corrected adiabatic triplet state energy for quinoline to be 2.69 eV at the CCSD/aug-cc-pVDZ level. The calculated triplet state energy is 0.1 eV lower than the triplet state energy from the gas phase phosphorescence spectrum, 2.79 eV,[7] and the calculations show the lowest triplet state to have a $^3(\pi^1\pi^{*1})$ electron configuration. Based on the mass spectrum, our experiments demonstrated formation of the quinoline-O_2 complex and following 312 nm photoexcitation we confirmed formation of $^1O_2$ through REMPI spectroscopy. We recorded the $^1O_2$ velocity map ion image, and from the resulting experimental $P(E_T)$, we determined the average quinoline internal energy to be 2.848 eV, which compares closely with the predicted average internal energy of 2.854 eV for statistical dissociation giving quinoline in the lowest triplet state and we considered several excitation mechanisms to account for these products. Finally, we observed no enhancement of $^1O_2$ production through photoexcitation at 266 nm, which indicates the second quinoline singlet excited state and the charge transfer state do not play a large role in forming photochemical $^1O_2$.

■ ASSOCIATED CONTENT

Supporting Information

The Supporting Information is available free of charge at https://pubs.acs.org/doi/10.1021/acs.jpca.3c02024.

Figure showing quinoline structure and structure of quinoline-O_2 complex, figures of singly occupied quinoline molecular orbitals, figure showing mass spectrum of molecular beam, figure showing the calculated prior distribution for dissociation giving ground state quinoline, tables of quinoline ground state and lowest triplet state geometry, tables of quinoline ground state and lowest triplet state harmonic frequencies, tables of quinoline-O_2 complex Cartesian coordinates and harmonic vibrational frequencies (PDF)

https://doi.org/10.1021/acs.jpca.3c02024
J. Phys. Chem. A 2023, 127, 4957−4963

AUTHOR INFORMATION

Corresponding Author

Bradley F. Parsons − *Department of Chemistry and Biochemistry, Creighton University, Omaha, Nebraska 68178, United States;* orcid.org/0000-0002-0749-8257; Phone: 402−280−3735; Email: bparsons@creighton.edu

Authors

Marcos R. Rivera − *Department of Chemistry and Biochemistry, Creighton University, Omaha, Nebraska 68178, United States*

Mark A. Freitag − *Department of Chemistry and Biochemistry, Creighton University, Omaha, Nebraska 68178, United States*

Kylie A. Reardon − *Department of Chemistry and Biochemistry, Creighton University, Omaha, Nebraska 68178, United States*

Emerson S. Pappas − *Department of Chemistry and Biochemistry, Creighton University, Omaha, Nebraska 68178, United States*

Jack T. Rausch − *Department of Chemistry and Biochemistry, Creighton University, Omaha, Nebraska 68178, United States*

Complete contact information is available at: https://pubs.acs.org/10.1021/acs.jpca.3c02024

Notes

The authors declare no competing financial interest.

ACKNOWLEDGMENTS

This work was supported by the National Science Foundation under grant number CHE-2150871. B.F.P. gratefully acknowledges financial assistance through a CURAS Summer Faculty Research Fellowship from the College of Arts and Sciences at Creighton University. We also gratefully thank Professor Kade Head-Marsden and Dr. Anthony Schlimgen for insightful conversations during the drafting of the manuscript.

REFERENCES

(1) Sutherland, D.; Compton, C. The Absorption Spectra of Some Substituted Quinolines and Their Methiodides. *J. Org. Chem.* **1952**, *17*, 1257−1261.

(2) Anton, M. F.; Moomaw, W. R. Luminescence and Hydrogen Bonding in Quinoline and Isoquinoline. *J. Chem. Phys.* **1977**, *66*, 1808−1818.

(3) Coppens, G.; Gillet, C.; Nasielski, J.; Vander Donckt, E. Physico-chemical Properties of Aromatic Compounds. IV. Effect of the Polarity of the Solvents on the N-V and n-π^* Transitions of Some Monoazaaromatic Derivatives. *Spectrochim. Acta* **1962**, *18*, 1441−1453.

(4) Leach, S.; Jones, N. C.; Hoffmann, S. V.; Un, S. VUV Absorption Spectra of Gas-Phase Quinoline in the 3.5-10.7 eV Photon Energy Range. *J. Phys. Chem. A* **2018**, *122*, 5832−5847.

(5) Innes, K. K.; Ross, I. G.; Moomaw, W. R. Electronic States of Azabenzenes and Azanaphthalenes: A Revised and Extended Critical Review. *J. Mol. Spectrosc.* **1988**, *132*, 492−544.

(6) Hiraya, A.; Achiba, Y.; Kimura, K.; Lim, E. C. Identification of the Lowest Energy nπ^* States in Gas-phase Polycyclic Monoazines: Quinoline and Isoquinoline. *J. Chem. Phys.* **1984**, *81*, 3345−3347.

(7) Okajima, S.; Lim, E. C. Radiationless Transitions in Gaseous Nitrogen Heterocyclics: Energy Dependence of Internal Conversion in Quinoline and Isoquinoline. *J. Chem. Phys.* **1978**, *69*, 1929−1933.

(8) Lim, E. C.; Yu, J. M. H. Vibronic Spin-orbit Interactions in Heteroaromatic Molecules. I. Polycyclic Monoazines. *J. Chem. Phys.* **1967**, *47*, 3270−3275.

(9) Harabuchi, Y.; Saita, K.; Maeda, S. Exploring Radiative and Nonradiative Decay Paths in Indole, Isoindole, Quinoline and Isoquinoline. *Photochem. Photobiol. Sci.* **2018**, *17*, 315−322.

(10) Lhiaubet-Vallet, V.; Miranda, M. A. Singlet Oxygen Generation by Drugs and Their Metabolites. In *Singlet Oxygen*; Royal Society of Chemistry: Cambridge, U.K., 2016; Vol. *I*, pp 287−303.

(11) Pretali, L.; Fasani, E.; Sturini, M. Current Advances on the Photocatalytic Degradation of Fluoroquinolones: Photoreaction Mechanism and Environmental Application. *Photochem. Photobiol. Sci.* **2022**, *21*, 899−912.

(12) Kolpin, D. W.; Furlong, E. T.; Meyer, M. T.; Thurman, E. M.; Zaugg, S. D.; Barber, L. B.; Buxton, H. T. Pharmaceuticals, Hormones, and Other Organic Wastewater Contaminants in U.S. Streams, 1999-2000: A National Reconnaissance. *Environ. Sci. Technol.* **2002**, *36*, 1202−1211.

(13) Albini, A.; Monti, S. Photophysics and Photochemistry of Fluoroquinolones. *Chem. Soc. Rev.* **2003**, *32*, 238−250.

(14) Martinez, L. J.; Sik, R. H.; Chignell, C. F. Fluoroquinolone Antimicrobials: Singlet Oxygen, Superoxide and Phototoxicity. *Photochem. Photobiol.* **1998**, *67*, 399−403.

(15) Baptista, M. S.; Cadet, J.; Mascio, P. D.; Ghogare, A. A.; Greer, A.; Hamblin, M. R.; Lorente, C.; Nunez, S. C.; Ribeiro, M. S.; Thomas, A. H.; et al. Type I and Type II Photosensitized Oxidation Reactions: Guidelines and Mechanistic Pathways. *Photochem. Photobiol.* **2017**, *93*, 912−919.

(16) Loeb, S.; Hofmann, R.; Kim, J. H. Beyond the Pipeline: Assessing the Efficiency Limits of Advanced Technologies for Solar Water Disinfection. *Environ. Sci. Technol. Lett.* **2016**, *3*, 73−80.

(17) Vidma, K. V.; Frederix, P. W. J. M.; Parker, D. H.; Baklanov, A. V. Photodissociation of van der Waals Clusters of Isoprene with Oxygen, C_5H_8-O_2 in the Wavelength Range 213-277 nm. *J. Chem. Phys.* **2012**, *137*, No. 054305.

(18) Baklanov, A. V.; Parker, D. H. Weakly Bound Environment of Molecular Oxygen as a Catalyst of Photooxidation. *Kinet. Catal.* **2020**, *61*, 174−197.

(19) Huber, K. P.; Herzberg, G. H. Constants of Diatomic Molecules. In *NIST Chemistry WebBook*, NIST Standard Reference Database Number 69; National Institute of Standards and Technology: Gaithersburg, MD, 2023. http://webbook.nist.gov.

(20) Thorning, F.; Strunge, K.; Jensen, F.; Ogilby, P. R. The Complex Between Molecular Oxygen and an Organic Molecule: Modeling Optical Transitions to the Intermolecular Charge-transfer State. *Phys. Chem. Chem. Phys.* **2021**, *23*, 15038−15048.

(21) Mulliken, R. S. Molecular Compounds and Their Spectra II. *J. Am. Chem. Soc.* **1952**, *74*, 811−824.

(22) Ervin, K. M.; Anusiewicz, I.; Skurski, P.; Simons, J.; Lineberger, W. C. The Only Stable State of O_2- Is the X $^2\Pi_g$ Ground State and It (Still!) Has an Adiabatic Electron Detachment Energy of 0.45 eV. *J. Phys. Chem. A* **2003**, *107*, 8521−8529.

(23) Barca, G. M. J.; Bertoni, C.; Carrington, L.; Datta, D.; De Silva, N.; Deustua, J. E.; Fedorov, D. G.; Gour, J. R.; Gunina, A. O.; Guidez, E.; et al. Recent Developments in the General Atomic and Molecular Electronic Structure System. *J. Chem. Phys.* **2020**, *152*, No. 154102.

(24) Neese, F. The ORCA Program System. *Wiley Interdiscip. Rev.: Comput. Mol. Sci.* **2012**, *2*, 73−78.

(25) Fletcher, G. D.; Schmidt, M. W.; Gordon, M. S. Developments in Parallel Electronic Structure Theory. *Adv. Chem. Phys.* **1999**, *110*, 267−294.

(26) Aikens, C. M.; Gordon, M. S. Parallel Unrestricted MP2 Analytic Gradients Using the Distributed Data Interface. *J. Phys. Chem. A* **2004**, *108*, 3103−3110.

(27) Dunning, T. H. Gaussian Basis Sets for Use in Correlated Molecular Calculations. I. The Atoms Boron Through Neon and Hydrogen. *J. Chem. Phys.* **1989**, *90*, 1007−1023.

(28) Piecuch, P.; Kucharski, S. A.; Kowalski, K.; Musial, M. Efficient Computer Implementation of the Renormalized Coupled-cluster Methods: The R-CCSD[T], R-CCSD(T), CR-CCSD[T], and CR-CCSD(T) Approaches. *Comput. Phys. Commun.* **2002**, *149*, 71−96.

(29) Even, U. The Even-Lavie Valve as a Source for High Intensity Supersonic Beam. *EPJ Tech. Instrum.* **2015**, *2*, No. 17.
(30) Even, U.; Jortner, J.; Noy, D.; Lavie, N.; Cossart-Magos, C. Cooling of Large Molecules Below 1 K and He Clusters Formation. *J. Chem. Phys.* **2000**, *112*, 8068−8071.
(31) Eppink, A. T. J. B.; Parker, D. H. Velocity Map Imaging of Ions and Electrons Using Electrostatic Lenses: Application in Photoelectron and Photofragment Ion Imaging of Molecular Oxygen. *Rev. Sci. Instrum.* **1997**, *68*, 3477−3484.
(32) Parsons, B. F.; Freitag, M. A.; Warder, H. J. Singlet O_2 Produced by Ultraviolet Excitation of the β-ionone-O_2 Complex. *J. Phys. Chem. A* **2021**, *125*, 8649−8657.
(33) Johnson, R. D.; Long, G. R.; Hudgens, J. W. Two Photon Resonance Enhanced Multiphoton Ionization Spectroscopy of Gas Phase O_2 a $^1\Delta_g$ Between 305-350 nm. *J. Chem. Phys.* **1987**, *87*, 1977−1981.
(34) Morrill, J. S.; Ginter, M. L.; Hwang, E. S.; Slanger, T. G.; Copeland, R. A.; Lewis, B. R.; Gibson, S. T. Two-photon REMPI Spectra from a $^1\Delta_g$ and b $^1\sum_g^+$ to d $^1\Pi_g$ in O_2. *J. Mol. Spectrosc.* **2003**, *219*, 200−216.
(35) Dribinski, V.; Ossadtchi, A.; Mandelshtam, V. A.; Reisler, H. Reconstruction of Abel-Transformable Images: The Gaussian Basis-set Expansion Abel Transform Method. *Rev. Sci. Instrum.* **2002**, *73*, 2634−2642.
(36) Eppink, A. T. J. B.; Parker, D. H. Methyl Iodide A-band Decomposition Study by Photofragment Velocity Imaging. *J. Chem. Phys.* **1998**, *109*, 4758−4767.
(37) Hadley, S. G. Direct Determination of Singlet → Triplet Intersystem Crossing Quantum Yield. II. Quinoline, Isoquinoline, and Quinoxaline. *J. Phys. Chem. A* **1971**, *75*, 2083−2086.
(38) Lim, E. C.; Yu, J. M. H. Vibronic Spin-orbit interactions in Heteroaromatic Molecules. II. Phosphorescence of Quinoxaline and Other Diazanaphthalenes. *J. Chem. Phys.* **1968**, *49*, 3878−3884.
(39) Western, C. M. PGOPHER: A Program for Simulating Rotational, Vibrational and Electronic Spectra. *J. Quant. Spectrosc. Radiat. Transfer* **2017**, *186*, 221−242.
(40) McDonald, J. D.; LeBreton, P. R.; Lee, Y. T.; Herschbach, D. R. Molecular Beam Kinetics: Reactions of Deuterium Atoms with Halogen Molecules. *J. Chem. Phys.* **1972**, *56*, 769−788.
(41) Holmes-Ross, H. L.; Lawrance, W. D. Anomalous Behavior in NO-Ar ($\tilde{A}$) Photodissociation Near Threshold: A Significant Contribution from Thermally Populated States. *Chem. Phys. Lett.* **2008**, *458*, 15−18.
(42) Urbain, P.; Leyh, B.; Remacle, F.; Lorquet, A. J.; Flammang, R.; Lorquet, J. C. Unimolecular Reaction Dynamics from Kinetic Energy Release Distributions. III. A Comparative Study of the Halogenobenzene Cations. *J. Chem. Phys.* **1999**, *110*, 2911−2921.
(43) Baer, T.; Hase, W. L. *Unimolecular Reaction Dynamics*; Oxford University Press: New York, NY, 1996.

https://doi.org/10.1021/acs.jpca.3c02024
J. Phys. Chem. A 2023, 127, 4957−4963